UNDERSTANDING AND MITIGATING THE LID IN SP Al-BSF Cz-Si SOLAR CELL BY USE OF IR-BELT FURNACE RAPID THERMAL PROCESSING

by

Mayangi Ma Mvutu

A thesis submitted to the faculty of
The University of North Carolina at Charlotte
in partial fulfillment of the requirements
for the degree of Master of Science in
Applied Energy and Electromechanical Systems

Charlotte

2016

Approved by:

____
Dr. Abasifreke Ebong

____
Dr. Maciej Noras

____
Dr. Yong Zhang

____
Dr. Barry Sherlock

____
Dr. Umit Cali

ABSTRACT

MAYANGI MA MVUTU. Understanding and mitigating the light-induced degradation in screen printed Al-BSF Cz-Si solar cell by use of IR-belt furnace Rapid Thermal Processing. (Under the direction of DR. ABASIFREKE EBONG)

In this study, Rapid Thermal Processing was used to understand and mitigate the light-induced degradation in boron-doped Cz-Si solar cells. Two different design-types of solar cells were used in the experiment to investigate the impact the solar cell design (structure) might have in lifetime recovery. The two design types include 5-Busbar (5BB) and 4-Street-5-Busbar (4S-5BB), with a resistivity of 2 Ω-cm, surface area of 239 cm^2, thickness of 0.018 cm, and doping concentration of 7.22×10^{15} cm^{-3}. In the annealing process, the peak temperature of 795°C, belt speed of 210 ipm, and dwell time of less than 2 minutes were used. It was found that solar cell design-type does not affect the lifetime recovery, since both design-types showed similar trends in all electrical output parameters. Also, although the lifetime was fully recovered following the annealing, the efficiency was not, because of contact degradation that resulted in high series resistance and junction recombination. Thus contact firing is key to effective lifetime and efficiency recovery.

DEDICATION

This work is dedicated to

my beloved wife, Nyamabu Annie Mvutu, for supporting and encouraging me through great sacrifices and love,

my children Emmanuel Bakitanga, Joseph Ilunga, Hannah Bafundila, and Elijah Tutinina-Mu-Yesu-Klisto Mvutu for joy, peace, and happiness they give me,

my mom Bafundila Therese Mayangi for always being available to help out every time help is needed.

ACKNOWLEDGMENTS

First of all, I owe my profound gratitude to the Lord Jesus-Christ for His grace and mercy which have provided me with wisdom and ability in this achievement.

I would like to express my sincere gratitude to my advisor, Dr. Abasifreke Ebong, for the incredible time commitment to guidance, support, and encouragement that have made this thesis possible, and for the productive research environment this has created. I would like to thank also, in a particular way, my other advisor in this work, Dr. Noras Maciej, for the diligence in providing me directions to face challenges throughout my Master's Degree studies. I would like to thank my committee members, Dr. Yong Zhang, for his experience and expertise in materials, Dr. Barry Sherlock and Dr. Umit Cali, for their individual contributions. I would like to thank Dr. Demba Ndiaye for proofreading this thesis.

I would like to thank also Dr. Ebong's research team (Yu-Chen HSU, Ahrar Chowdhury, and Veysel Unsur) at photovoltaic research laboratory (PVRL), in energy production and infrastructure center (EPIC), at UNC Charlotte for the assistance obtained in the use of different laboratory equipment. In particular, my sincere gratitude to Yu-Chen HSU, for her tremendous efforts and interest to see that my research was done right and on time.

Finally, I would like to thank my wife, Nyamabu A. Mvutu, for her sacrifices, patience, and confidence in support of this research through the moments of great challenges.

TABLE OF CONTENTS

LIST OF TABLES

LIST OF FIGURES

CHAPTER 1: PHOTOVOLTAICS

1.1. Introduction

The conventional energy source reserves are rapidly depleting. Based on 2005 estimations, depletion times for oil, natural gas, and coal have been approximated to 35, 107, and 37 years, respectively [1]. In addition, their associated environmentally unfriendly effects continue to grow concerns among the developed countries. Researches are being conducted to find environmentally friendly and sustainable alternatives to fossil fuels. Increased attention is being given to renewable sources of energy including wind, geothermal, ocean, biofuel, and solar energy [2-4].

The world primary energy consumption in 2015 was 13,147.3 Mtoe [5]. This is equivalent to the power consumption of 1.746 x 10^{13} W (1 Mtoe = 11.631 x 10^{12} Wh) for the same year. The total solar flux that is absorbed at sea level is approximated at 1.2 x 10^{17} W [6]. The sun has therefore the potential to supply 6,872.85 times the average world power consumption of 2015.

1.2. Brief History of PV

A solar cell is a semiconductor device which converts solar radiation directly into electricity by the photovoltaic effect.

Photovoltaic (PV) effect is a process that generates voltage in a solar cell. It was first discovered by Edmund Becquerel in 1839, with very limited device applications [7]. The advent of silicon as the prime semiconductor material, about a century later, has broadened the field for the PV applications. Silicon-based solar cell invented in 1954 played an important role during the 1960s' space competition between the United States of America and Soviet Union [8]. In the quest for lower production costs and higher efficiency, solar cell technology has evolved through three generations. The first generation is predominant on the market; it is known as silicon wafer-based. The second generation aimed to reduce the costs involved in the solar cell's materials by utilizing the thin film technology [9]. The third generation, however, is exploring possibilities to achieve higher efficiencies. It has been suggested that solar cells performance could be improved 2-3 times, given that different fundamentals concepts were used in the design of the third generation [9].

1.3. Conversion of Sunlight into Electricity Utilizing Solar Cells

1.3.1. Contributing Factors to Solar Cell Operation

The conversion of solar energy into electricity utilizing photovoltaics (PV) is achieved through the process of absorption of incident photons, generation of electron-hole pairs, and separation of electrons and holes, and collection of these carriers at the respective contacts.

Ideally, the incident photons from the sun are absorbed into the bulk material (base) of the solar cell, which usually is made of n- or p-type for a single junction solar cell. However, only photons with energy (E_{ph}) equal to the material's bandgap energy (E_g) would be absorbed. Photons with energy greater than, or less than, the material's bandgap energy ($E_{ph} > E_g$ or $E_{ph} > E_g$) constitute a loss in solar cell. These losses are further discussed in the next section, solar cell's performance limiting mechanisms, under optical losses. In addition, part of the incident photons would be reflected back and not be absorbed. The absorbed photons in the base of the solar cell participate to electron-hole pair generation. The presence of electric field in the solar cell created by the dissimilar materials, n-type and p-type, causes the separation of carriers such that electrons are attracted towards the n-type, to the front contact, and the holes towards the p-type, to the rear contact.

Fig. 1 shows a general structure of a p-type, single junction solar cell. It also illustrates the basic process of the operation of a solar cell, including absorption (and reflection) of incident photons, generation, and separation of electron-hole pairs.

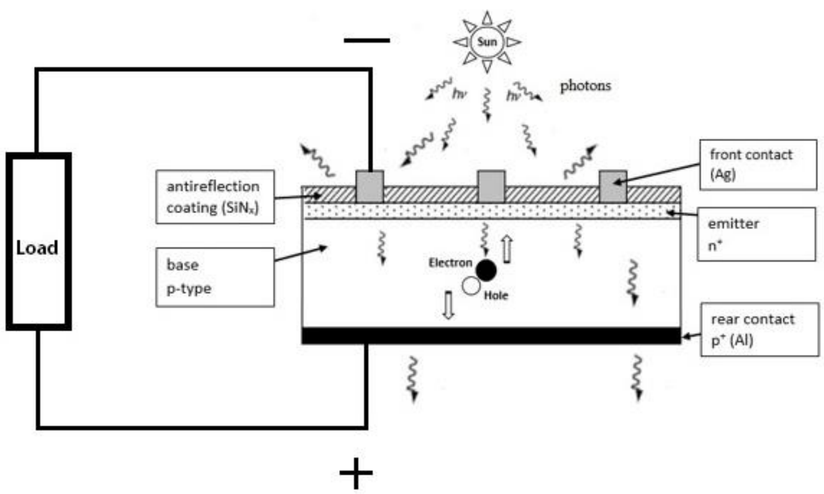

Figure 1: Basic structure of a single junction p-type solar cell and solar energy conversion to electricity

The conversion process of solar energy to electric power is accomplished when carriers collected at the contacts find a path to an external load, as illustrated in Fig. 1.

1.3.2. Electrical Output Parameters of a Solar Cell

When a solar cell is not illuminated (or in the “dark”), as a p-n junction semiconductor device, it behaves like a simple diode, as illustrated in Fig. 2 (a).

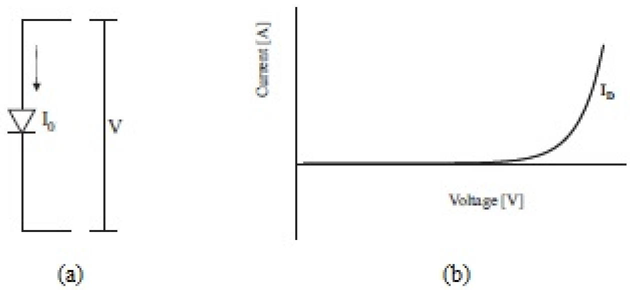

Figure 2: (a) A simplified one-diode model of a solar cell – not illuminated, (b) I-V curve

The current-voltage characteristic curve for such device is shown in Fig. 2 (b), and is described by the equation (1) [10].

$$(I\text{-}V) \quad I_D = I_0 \left[\exp\left(\frac{qV}{nkT}\right) - 1\right] \tag{1}$$

Where I_D is the diode current, I_0 is the reverse saturation current of the diode, q is the electric charge of an electron (1.602×10^{-19} C), V is the voltage across the diode, n is the ideality factor, k is the Boltzmann constant (1.38×10^{-23} J/K), and T is the junction temperature.

The illumination of the solar cell, as depicted in Fig. 3 (a), causes the photo-generated current to rise and the I-V curve to have a vertical translation to the fourth quadrant, as illustrated in Fig. 3 (b) and described by the equations (2) and (3).

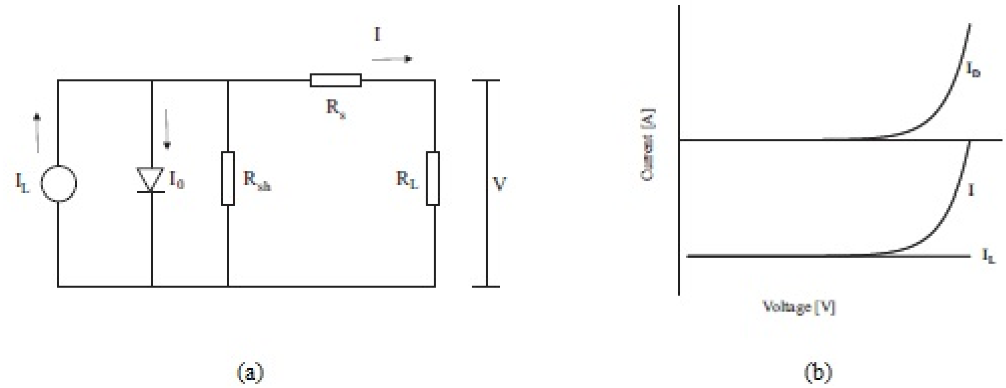

Figure 3: (a) The illuminated one-diode model of a solar cell and
(b) I-V characteristic curve

$$I = I_L - I_D \tag{2}$$

$$I = I_L - I_0\left[\exp\left(\frac{qV}{nkT}\right) - 1\right] \tag{3}$$

Where I and I_L are the solar cell output current and the photo-generated current, respectively, and I_0 the reverse saturation current, and q, V, n, k, and *T* represent the same parameters as in equation (1). The circuit in Fig. 3 (a) illustrates the illuminated solar cell, where, in addition to parameters shown in Fig. 2 (a), R_s is the series resistance, R_{sh} is the shunt resistance, and R_L is the load. Resistive effects (R_s & R_{sh}) or parasitic resistances affect the fill factor, and therefore the efficiency of the solar cell.

The one-diode model of solar cell used here, as shown in Fig. 3, is more theoretical than practical. In this model, several practical aspects of solar cell are not taken into account including junction recombination. The two-diode model of a solar cell, Fig. 4 - well discussed in the literature, is considered more realistic since it captures the junction recombination effects [10].

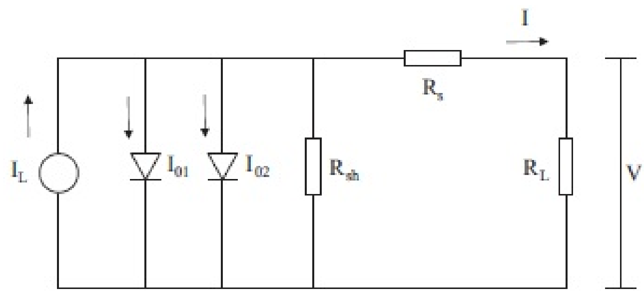

Figure 4: illuminated two-diode model of a solar cell

$$I = I_L - I_{01}\left[\exp\left(\frac{q(V+IR_s)}{kT}\right)-1\right] - I_{02}\left[\exp\left(\frac{q(V+IR_s)}{2kT}\right)-1\right] - \frac{V-IR_s}{R_{shunt}} \tag{4}$$

In this case, the junction recombination, which was not taken into account in the one-diode model shown in Fig. 3, is now modeled using I_{o2}, as shown in Fig. 4 and used in equation (4).

The electrical power is generated by the current and voltage produced by photovoltaic effect due to the incident light on the solar cell. The performance of a solar cell can be characterized by several important parameters, including short-circuit current, open-circuit voltage, and fill factor.

a. Short-Circuit Current (I_{sc})

The short-circuit current of a solar cell is a function of the surface area, the number of photons absorbed, the spectrum of the incident light, the optical properties of the solar cell, and the collection probability. The short-circuit current is the output current of the solar cell when the voltage is zero (I_{sc} = I, V = 0). It is illustrated in Fig. 5.

b. Open-Circuit Voltage (V_{oc})

The open-circuit voltage is the maximum output voltage of a solar cell. Similar to I_{sc}, V_{oc} is the output voltage of the solar cell when the short-circuit current is zero (V_{oc} = V, I_{sc} = 0), as shown in Fig. 5.

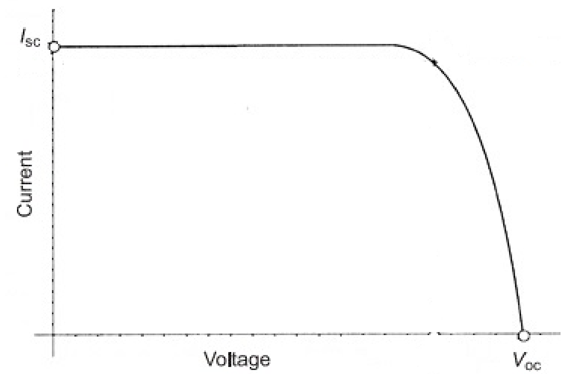

Figure 5: I-V Characteristic curve – V_{oc} and I_{sc}

c. Fill Factor (FF)

The fill factor is the ratio of the maximum power (V_m x I_m) to the theoretical power (V_{oc} x I_{sc}), as graphically illustrated in Fig. 6.

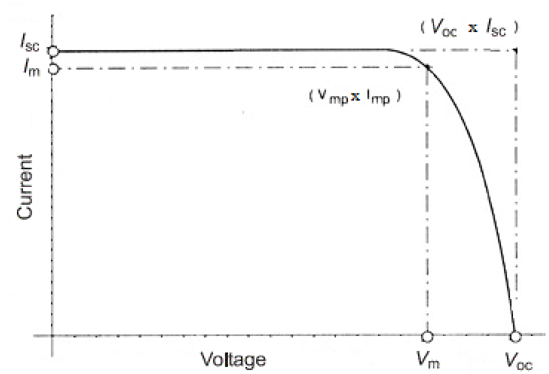

Figure 6: I-V Characteristic curve – FF

The fill factor is also the measure of "squareness" of the *I-V* curve, as shown in Fig. 6.

Mathematically, FF is given by equation (5), as follows:

$$FF = \frac{V_m \, x \, I_m}{V_{oc} \, x \, I_{sc}} \tag{5}$$

Where V_m and I_m are maximum voltage and maximum current, respectively.

d. Efficiency (η)

The efficiency is the figure of merit of a solar cell. Mathematically, it is calculated by dividing the output power (P_{out}) of the solar cell by the input power (P_{in}) from the sun, as shown in equation (6).

$$\eta\ (\%) = \frac{P_{out}}{P_{in}}\, x\ 100 \tag{6}$$

Usually, for calculation purpose, the input power is estimated to be 1 kW/m^2, also called 1 sun illumination. The fill factor (FF), in conjunction with the open-circuit voltage (V_{oc}) and the short-circuit current (I_{sc}), determines the output power. The equation (6) can therefore be written as in (7).

$$\eta\ (\%) = V_{oc}\ x\ I_{sc}\ x\ FF \tag{7}$$

1.4. Solar Cell's Performance Limiting Mechanisms

Loss mechanisms affecting the efficiency of a solar cell include optical and electrical parameters.

1.4.1. Optical

A large number of incident photons on a solar cell are not absorbed due to the bandgap of the material. The efficiency is largely reduced based on this limitation.

For the photons with energy greater than the bandgap energy of the material ($h\upsilon > E_G$), only the part that is equal to the bandgap energy would be absorbed and the excess energy would be lost, or dissipated as heat. For silicon material, with a bandgap energy of 1.12 eV, this loss is approximated to about 29% of the incident energy at 1 sun radiation, or AM1.5 Global [11].

Similarly, photons with energy less than the bandgap energy of the material (hυ < EG), would not be absorbed and would result to a loss. Silicon material accounts for about 23% loss of this type [11].

Fig. 7 shows the maximum efficiency of solar cells based on the band gap material for radiation of 1 sun/1000 suns (300K).

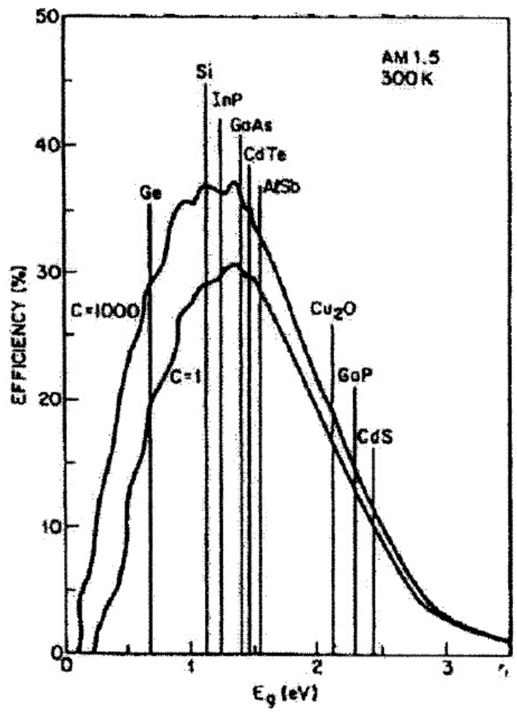

Figure 7: Maximum solar cell efficiency
for radiation of 1 sun/1000 suns
versus energy band gap of materials [12].

In addition, incomplete absorption is considered when the width of the material is less than 1/α, where α is the absorption coefficient of the material. Reflection of incident photons and solar cell shadowing constitute other forms of energy loss [11].

1.4.2. Electrical

Electrical losses can be of Ohmic or recombination type, or both.

A. Ohmic Losses

Losses related to the semiconductor material (base and emitter) and contact material (gridlines, collection bus, and metal-semiconductor junction) are considered Ohmic, as shown in Fig. 8 (a) and (b).

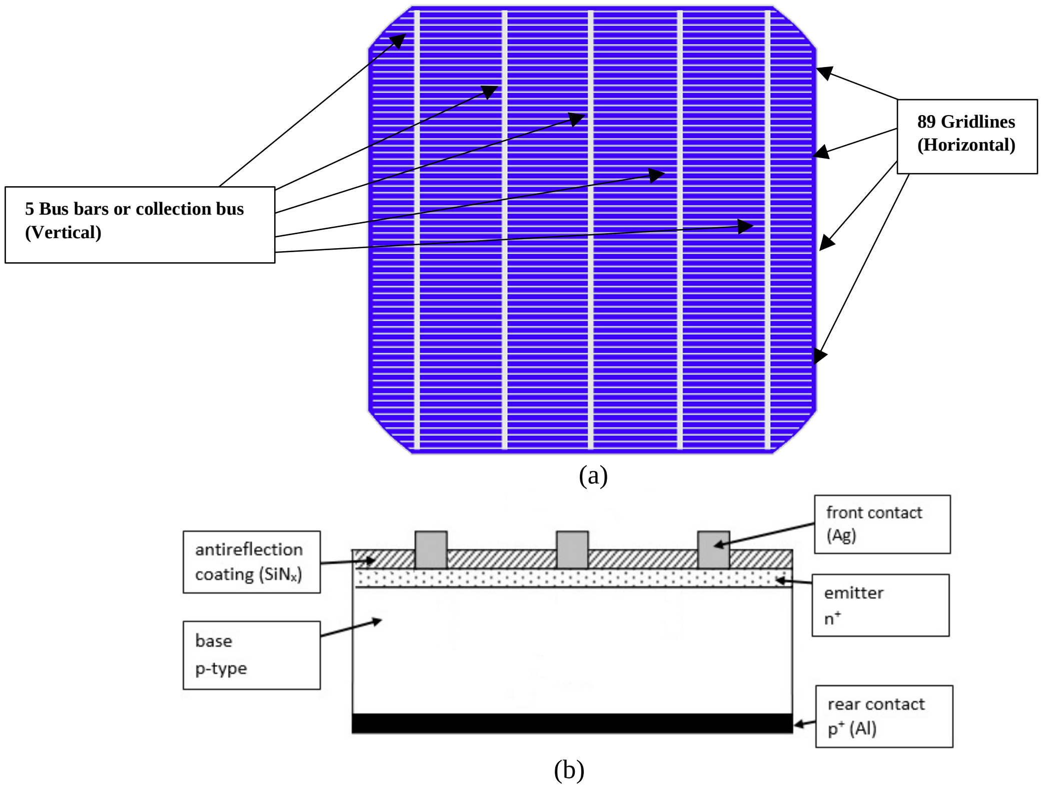

Figure 8: (a) Top view of a solar cell showing fingers & bus-bars
(b) Side view of a solar cell depicting a screen-printed single-junction structure

B. Recombination Losses

Losses can occur in the emitter region (surface), the bulk or base region (semiconductor material), or the space charge region of the solar cell through a mechanism termed carrier recombination. Recombination reduces the number of carriers in the semiconductor material and limit the amount of carriers that would contribute to current. It is therefore detrimental to short-circuit current as well as open-circuit voltage. The three main types of carrier recombination in a solar cell include bulk recombination, surface recombination, and depletion region recombination. They are named based on the location of the solar cell where they occur.

The surface and the bulk are the locations of a solar cell where carriers recombination occur the most. Much consideration is required in the design of a solar cell to minimize the recombination in these areas and optimize the prospect to achieve high efficiency.

B.1. Surface Recombination

Surface recombination velocity (S) is used in the analysis of surface recombination rather than carrier lifetime because of the type of states present at this location. Parameters affecting surface recombination velocity include the doping concentration, dopant type, diffusion, surface texturing, and chemical passivation [13].

B.2. Bulk Recombination

The bulk recombination is described based on (a) the material bandgap type (direct or indirect), (b) the level of external excitation applied (light – under illumination or voltage – under forward bias, also said in the dark), (c) and the impurities present in the bulk material. Fig. 9 shows the three recombination types: (a) Radiative, (b) Shockley-Read-Hall, and (c) Auger.

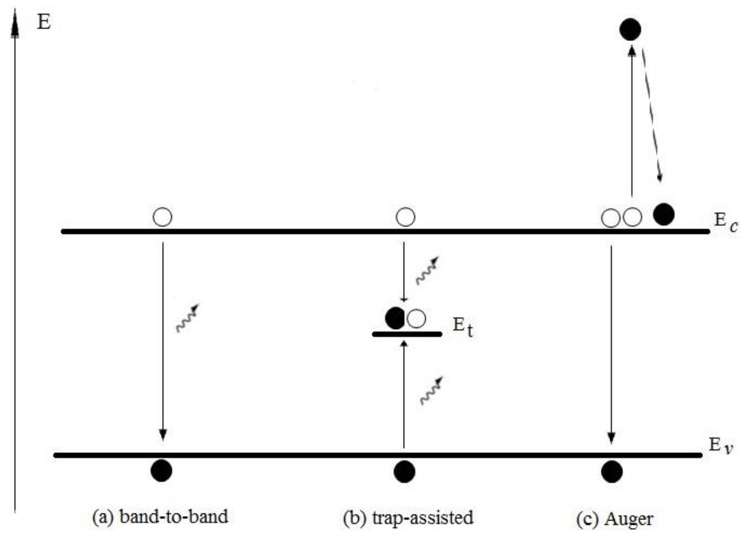

Figure 9: Types of bulk recombination:
(a) Radiative, (b) Shockley-Read-Haul, and (c) Auger

Bulk lifetime is given mathematically by the equation (8) as follows,

$$\frac{1}{\tau_{bulk}} = \frac{1}{\tau_{radiative}} + \frac{1}{\tau_{SHR}} + \frac{1}{\tau_{auger}} \tag{8}$$

As illustrated in Fig. 9, radiative recombination is of band-to-band type. It consists of an electron in the conduction band which loses energy and falls down to the valence band to recombine with a hole. Since silicon is an indirect bandgap material, the radiative recombination is almost inexistent and negligible. The Shockley-Read-Hall (SRH) recombination is a trap-assisted. The presence of impurities or defects in the material creates states or recombination centers in the forbidden gap. These centers will cause electrons from conduction band and holes from the valence band to be trapped in recombination. Auger recombination requires two electrons in the conduction band. One electron gives up energy, and while falling down to the valence band, the released energy promotes the other electron to a higher energy state in the conduction band before it relaxes back down to its lower initial energy state in the conduction band.

The carrier effective lifetime (τ_{eff}) in solar cell takes into consideration both types of recombination discussed above, the bulk and the surface. Mathematically, it is given as shown in equation (9).

$$\frac{1}{\tau_{eff}} = \frac{1}{\tau_{bulk}} + \frac{S_{front}+S_{rear}}{W} \tag{9}$$

Where τ_{eff} is the effective lifetime, τ_{bulk} is the bulk lifetime, W is the thickness of the solar cell sample, and S_{front} and S_{rear} are the front and rear surface recombination velocities, respectively.

1.5. Motivation

1.5.1. Introduction

Carrier recombination in the bulk material via traps sets the stage for the work presented in this study. Despite the quality of the solar cell design, the level of impurity in the material, or the degree of defect, the incident light on the solar cell creates recombination centers in the semiconductor bulk material. This is more observed in the boron-doped Cz-Si solar cells. These traps reduce carrier lifetime and are found to degrade the efficiency of the solar cell by 10% [13]. Mitigating LID in boron-doped Cz-Si solar cells is therefore critical in stabilizing the achieved efficiency.

1.5.2. Importance of Cz-Si Solar Cells among Crystalline Silicon Solar Cells

Boron-doped Cz-Si solar cells suffer initial efficiency degradation due to metastable defect upon illumination, as well as during carriers’ injection (forward bias).

Silicon is known to be the material of choice in the semiconductor industry, whether for electronics or photovoltaics (PV) applications. In photovoltaics for instance, according to [13], boron-doped crystalline silicon accounts for 93% of solar cell types produced in the world. Three types of silicon growth techniques contribute to that figure, 36% of Czochralski mono-crystalline silicon (Cz-Si), 52% of block-cast multi-crystalline silicon (mc-Si), and 5% of ribbon-grown Si sheets [13]. Although Cz-Si provides higher efficiencies than mc, the preference of the block-cast mc-Si over Cz-Si may be in the fact that mc-Si is less expensive to produce and LID is very low.

Material type	World Photovoltaic (PV) market share
Crystalline Silicon (c-Si)	90%
others	10%

Technology type	Crystalline Silicon (c-Si) solar cells
Czochralski Silicon (Cz-Si)	40%
Others	60%

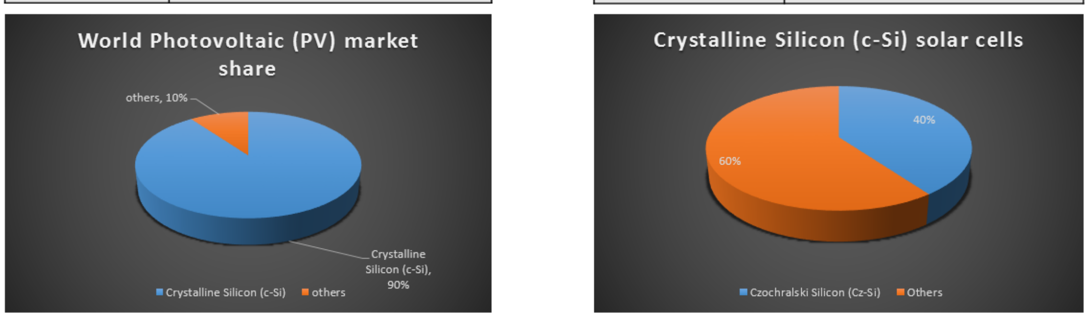

(a) (b)

Figure 10: (a) Crystalline Silicon solar cell status in PV market,
(b) Czokralski Silicon solar cells position among crystalline solar cells

The PV industry, in general, has been striving to achieve higher solar cell efficiencies and to lower overall production costs to be more competitive. For instance, low oxygen concentration silicon grown using float zone (FZ) technique can provide even higher efficiencies (24.7%) than Cz-Si (19 – 20%); however, it is less favored because of its higher production costs [14]. Fig. 10 illustrates the importance of Cz-Si solar cells in the PV industry.

Therefore, improving the efficiency of the fairly inexpensive Cz-Si would make a significant impact to the industry.

CHAPTER 2: LITERATURE REVIEW ON LID

2.1. Introduction

The phenomenon called LID has been one of the major issues affecting the efficiency of boron-doped Cz-Si solar cells. It consists of recombination centers created by boron-oxygen pairs in the base material of boron-doped solar cell due to the incident light on the solar cell. The following section gives a chronological review on LID.

2.2. Chronological Review of LID

R.L. Crabb was the first to observe Light Induced Degradation (LID) in 1972 while investigating UV degradation of the coverslip for space solar cells [14]. However, in 1973, Fischer and Schunder attributed the decrease in solar cell output to carriers lifetime decay [15]. The degradation observed on 1 Ohm-cm boron doped Czochralski solar cell occurred during the first few hours the cell was exposed to light before it was stabilized. In addition, a possibility to completely recover the lost efficiency was found through a low temperature annealing process, at 200°C [15].

During the years between 1978 and 1996, several attempts were made by scholars to model the defect due to LID. These attempts resulted to different proposed models, mostly related to some metallic impurities such as complex of a lattice defect and a silver atom [16], possible dissociation of donor-acceptor defect pairs caused by excess carriers through recombination-enhanced mechanism [17], iron contamination levels [18], etc.

It was not until 1997 when Schmidt et al. [19] associated the degraded lifetimes of illuminated boron-doped Cz-Si (1 Ω-cm) to the formation of interstitial boron-oxygen pairs, apart from metallic impurities for the first time. A year later, in 1998, Glunz et al. [20] confirmed Schmidt et al.'s findings.

In 2000, Schmidt and Cuevas used the combination of injection level dependence of carrier lifetime change with Shockley-Read-Hall's theory to identify the electronic properties of the recombination center created during illumination with energy level between Ev+0.35 and Ec-0.45 eV and τ_{no}/τ_{po} between 0.1 and 0.2. This deep-level center was attributed to a new type of boron-oxygen complex (BO_n with $n \approx 5$) [21].

In this experiment, three B-doped Cz grown silicon starting materials were utilized to see the effect on lifetime after FGA annealing (700 – 800°C, 750°C optimal), for 30 to 90 s (60 s optimal) by Plasma-Enhanced Chemical Vapor Deposition (PECVD) hydrogenation (SiN, 10-20 % atomic hydrogen), Fig. 11 illustrates the results.

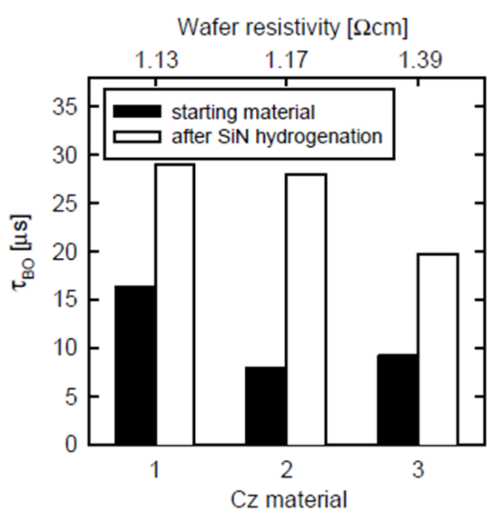

Figure 11: Effect of wafer resistivity on lifetime of materials
Before and after hydrogenation [21]

The same year, Saitoh et al. investigated LID mechanism and provided two main solutions to eliminate the defect: either reduce the boron and oxygen concentration or substitute boron by gallium as dopant [22].

Glunz et al. in 2001 suggested two solutions to LID as well, the use of gallium-doped Cz-Si, or the introduction of high-temperature anneals into the process sequence (conventional tube or rapid thermal processing) which would improve the carrier lifetime by a factor of 2 – 3 [23].

Vu et al. observed, in 2002, that boron-oxygen related defects in boron-doped Cz-Si solar cells vanish by thermal annealing at 200°C for 20 minutes [24]. It was Jan Schmidt in 2004 who gave the current understanding of the defect, an overview of defect models, and different approaches to avoid or reduce it [25]. Damiani studied LID through traps formation in combination with traps annihilation, finding possible recovery by trap dissociation and elevated temperatures [13].

In 2009 and 2010, Lim et al. observed that illumination at elevated temperature could permanently deactivate the boron-oxygen recombination centers [26, 27]. However, the defect reactions leading to such deactivation remain unresolved, but suggest that oxygen is involved in the deactivation process. Kang et al. showed in 2011 that LID in B-doped Cz solar cells, also depends on the Carbon content of the SiCxNy Anti Reflectance (AR) coating. SiNx AR coated solar cells suffer higher loss (0.3%) due to LID than SiCsNy AR coated solar cells (0.1%) [28].

Sopori et al. observed that LID in c-Si and mc-Si solar cells have two components: surface and bulk components. Bulk effect is Boron-Oxygen related (function of minority-carrier lifetime), which can be fully recovered through annealing. Surface effect, on the other hand, is SiN:H/Si interface related; for which the manifestation on the cell characteristics is very little, but easily seen in the J_{o2} component of the dark plot [29].

Ebong et al. observed LID to depend on belt speed and contact firing. In his study, the belt speed was found to be inversely proportional to the degradation level; while the ideality factor was proportional to the degradation level (e.g. cells fired at 250 IPM with n-factor of 1.06 showed lower LID than commercial grade cell having 1.10 n-factor) [30].

The following table and figures show the effect of belt speed on the fired multi-crystalline solar cells (~750°C peak firing temperature) as studied by [30].

CHAPTER 3: EXPERIMENTAL

3.1. Approaches/Methodology

The methodology used in this study consists of: (i) taking initial measurements of electrical output parameters of 7 finished solar cells, consisted of 4 samples of 4-street-5busbar (4S-5BB) and 3 samples of 5-busbar (5BB) designs, for reference by using the I-V tester and Suns-Voc, (ii) exposing those samples to solar radiation for 17 hours for degradation, (iii) measuring the solar cell electrical outputs every 30 minutes to monitor the degradation, (iv) annealing the samples using the IR belt-furnace RTP for recovery, at 795°C peak temperature for less than 2 seconds dwell time and a speed belt of 210 ipm, (v) measuring the solar cell electrical outputs immediately after the RTP anneal to monitor the recovery, (vi) exposing the samples to solar radiation afterwards to ensure the stability, and finally, (vii) measuring the solar cell electrical outputs every 30 minutes to verify if the stability of the efficiency has been achieved.

3.2. Experiment Layout - Set Up

3.2.1. Degradation

I-V tester (Sinton Instruments FCT-350) shown in Fig. 12 (a) and Suns-Voc (Sinton Instruments WCT-120) shown in Fig. 12 (b) were used to measure electrical output parameters (lifetime, Voc, Isc, FF, efficiency, etc.) before and after the exposition of solar cell samples directly to the sunlight. Depending on the time of the day, the weather (wind speed and direction, cloud, etc.), and location used for exposition, solar cell samples were constantly moved around to avoid any type of shading, and to ensure optimal incident sunlight throughout the exposition time.

Fig. 13 shows solar cells degradation under the sunlight, using 4 solar cell samples of 3 bus-bar design type (not used in this experiment) at a time.

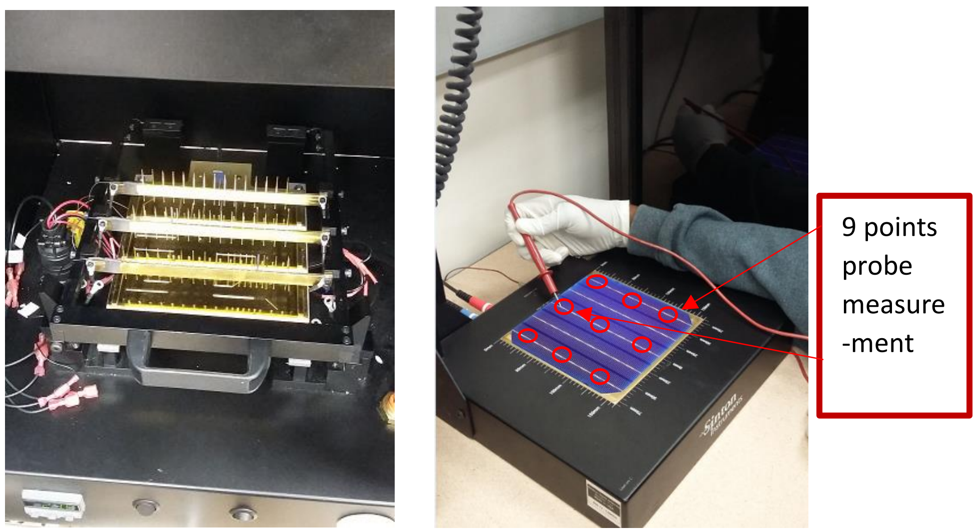

(a) (b)

Figure 12: Solar cell characterization using (a) I-V tester and (b) Suns-Voc

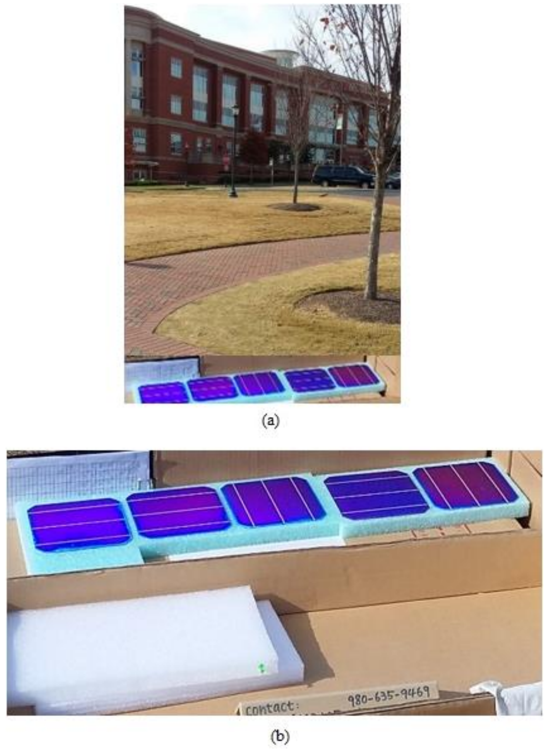

Figure 13: Lifetime degradation under 1 sun (AM1.5G)

3.2.2. Annealing

Data in Table 1 was recorded during the contact firing of the solar cell samples used in this experiment. They serve as reference in the comparison between contact firing and annealing temperature profiles.

Table 1: Contact firing profile data
of solar cells used in the experiment

Cell design	4S-5BB				5BB		
Cell ID#	001	002	005	006	003	005	015
Belt speed (ipm)	260	215	205	210	210	260	210
Peak temp. (°C)	780	780	780	780	780	780	780

Fig. 14 (c) shows the annealing profile used in this study. It also illustrates different phases of the RTP during solar cell annealing process.

Mitigation of LID in this study is accomplished utilizing RTP’s high temperature anneal capabilities to passivate boron-oxygen pairs, which constitute recombination centers in the solar cell.

Silicon nitride (SiNx) in the anti-reflection coating (ARC) serves as surface passivation. Inside the RTP furnace, at peak temperature of 795°C, and for a short dwell time of less than 2 seconds, SiNx undergoes chemical reaction and releases hydrogen (Si_xN_y:H). The released hydrogen serves to passivate recombination centers in the material. The fast ramp-up followed by the fast ramp-down enables the retention of hydrogen in the recombination center – hydrogen passivation.

(a) facing the furnace exit

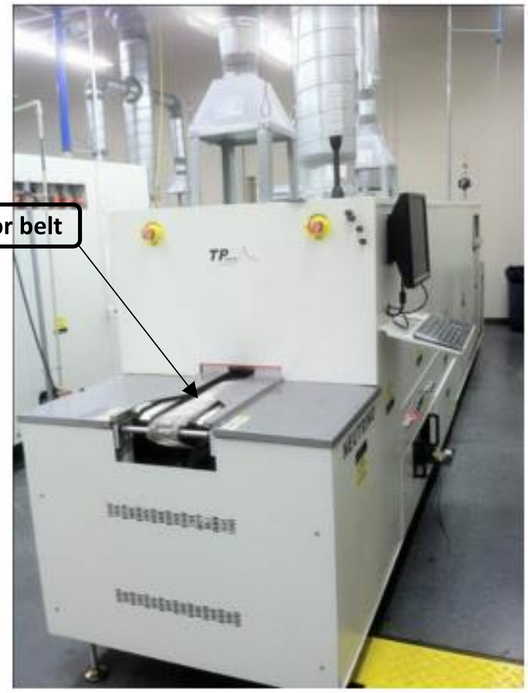

(b) facing the furnace entrance

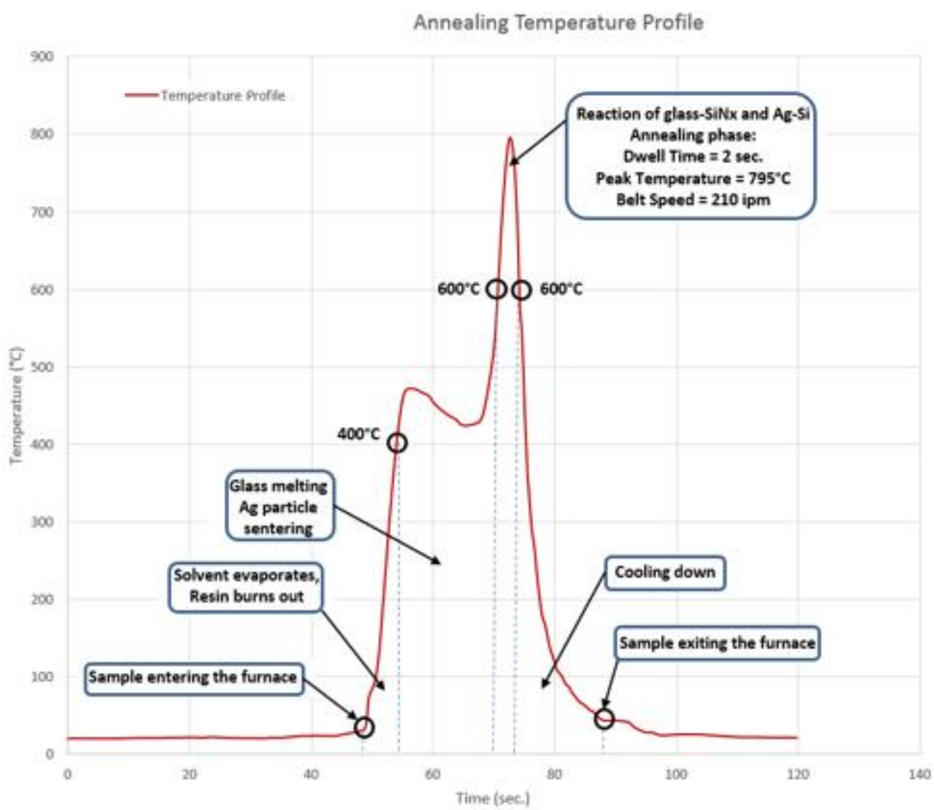

(c) Annealing temperature profile

Figure 14: Rapid Thermal Processing and Annealing Temperature Profile

CHAPTER 4: RESULTS AND DISCUSSION

4.1. Results

Tables 2 and 3 summarize electrical output parameters for the sets of solar cell designs before and after LID study.

Table 2: Pre-degradation parameters set up for solar cells used in the experiment

Pre-LID solar cell's parameter values							
	4 Street - 5 Busbars (4S-5BB)				5 Busbars (5BB)		
Cell ID	# 001	# 002	# 005	# 006	# 003	# 005	# 015
Parameters	Values	Values	Values	Values	Values	Values	Values
Resistivity (Ω-cm)	2	2	2	2	2	2	2
Cell Area (cm^2)	239	239	239	239	239	239	239
Thickness (cm)	0.018	0.018	0.018	0.018	0.018	0.018	0.018
Doping (cm^{-3})	7.22E+15	7.22E+15	7.22E+15	7.22E+15	7.22E+15	7.22E+15	7.22E+15
Doping type	p-type	p-type	p-type	p-type	p-type	p-type	p-type
Bulk Lifetime (µs)	59.67	55.6	54.23	57.33	51.4	61.18	60.61
Emitter (Ω/sq.)	100	100	100	100	100	100	100
FSRV (cm/s)	40000	40000	40000	40000	40000	40000	40000
BSRV (cm/s)	240	240	240	240	240	240	240
BSR (%)	71	71	71	71	71	71	71
R_{Series} (Ω-cm^2)	0.8587	0.8584	0.8696	0.8067	1.391961	1.208401	2.04195
R_{shunt} (Ω-cm^2)	large	large	large	large	large	large	large
J_{o1} (nA/cm^2)	1.00E-13	1.00E-13	1.00E-13	1.00E-13	1.00E-13	1.00E-13	1.00E-13
J_{o2} (nA/cm^2)	10.05	13.76	11.7	14.89	11.27	11.27	4.18
Efficiency (%)	18.58	18.42	18.53	18.59	17.78	18.22	17.44
V_{oc} (mV)	0.64	0.64	0.6395	0.64089	0.636852	0.639995	0.641095
J_{sc} (mA/cm^2)	0.037338	0.037051	0.037178	0.037084	0.036993	0.037034	0.036982
FF (%)	78.21	77.61	77.96	78.2	75.46	76.87	73.57
Ideality Factor (n)	1.079	1.103	1.089	1.097	1.118	1.092	1.064

$$R_s = \frac{V_{oc} * J_{sc} * (pFF - FF)}{{J_{mp}}^2} \tag{10}$$

Equation (10) is an empirical parameterization, obtained by [31], it is used in this study to calculate the series resistance recorded in Tables 2 and 3.

Table 3: Post-annealing parameters set up for solar cells used in the experiment

Post-Annealing solar cell's parameter values							
	4 Street - 5 Busbars (4S-5BB)				**5 Busbars (5BB)**		
Cell ID	**# 001**	**# 002**	**# 005**	**# 006**	**# 003**	**# 005**	**# 015**
Parameters	Values	Values	Values	Values	Values	Values	Values
Resistivity (Ω-cm)	2	2	2	2	2	2	2
Cell Area (cm^2)	239	239	239	239	239	239	239
Thickness (cm)	0.018	0.018	0.018	0.018	0.018	0.018	0.018
Doping (cm^{-3})	7.22E+15	7.22E+15	7.22E+15	7.22E+15	7.22E+15	7.22E+15	7.22E+15
Doping type	p-type	p-type	p-type	p-type	p-type	p-type	p-type
Bulk Lifetime (us)	50.72	46.64	47.5	48.6	52.7	52.02	57.7
Emitter (Ω/sq.)	100	100	100	100	100	100	100
FSRV (cm/s)	40000	40000	40000	40000	40000	40000	40000
BSRV (cm/s)	240	240	240	240	240	240	240
BSR (%)	71	71	71	71	71	71	71
R_{Series} (Ω-cm^2)	1.183247652	1.148901	1.988992751	0.995202013	2.116817	3.377947	3.535854
R_{shunt} (Ω-cm^2)	large	large	large	large	large	large	large
J_{o1} (nA/cm^2)	1.00E-13	1.00E-13	1.00E-13	1.00E-13	1.00E-13	1.00E-13	1.00E-13
J_{o2} (nA/cm^2)	19.91	31.06	20.48	20.29	12.04	13.03	9.77
Efficiency (%)	17.92	17.53	17.0051221	18.0243	16.94924	15.83545	15.70622
V_{oc} (mV)	0.638351891	0.636413	0.635799117	0.636715031	0.635939	0.635699	0.636813
J_{sc} (mA/cm^2)	0.03704	0.036824	0.03706803	0.036987521	0.03686	0.036694	0.036259
FF (%)	75.7701801	74.79423	72.1526858	76.53	72.30632	67.88708	68.02108
Ideality Factor (n)	1.160610833	1.22656	1.148169966	1.1681	1.148096	1.14043	1.125727

The effective lifetime for the solar cells, not recorded in Tables 2 and 3, was calculated to be about 202 µs by using equation (9), repeated here, as follows:

$$\frac{1}{\tau_{eff}} = \frac{1}{\tau_{bulk}} + \frac{S_{front} + S_{rear}}{W} \tag{11}$$

Figs. 15 and 16 show the efficiency trending with exposure time every 30 minutes for 18 hours. They also show the efficiency after 795°C anneal for less than 2 seconds and post-stability exposure for 2 hours.

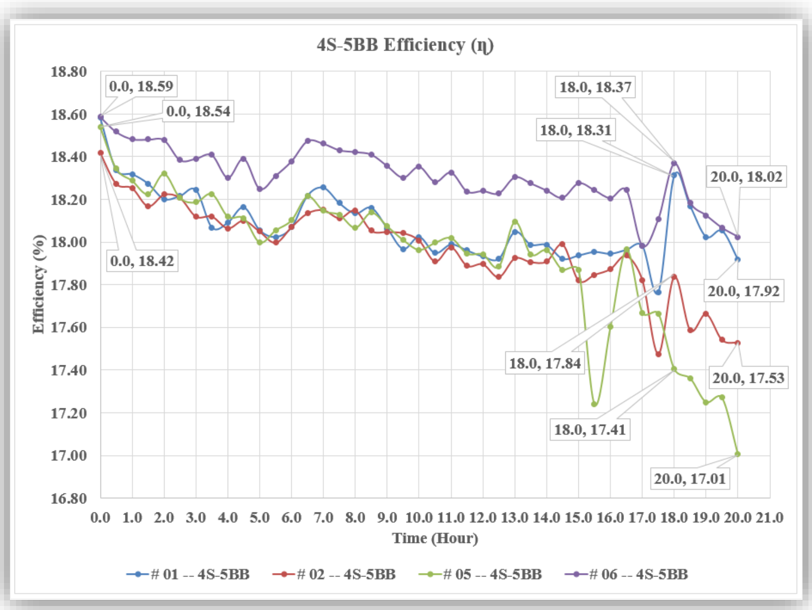

Figure 15: Efficiency curves for all the 4S-5BB solar cell design type

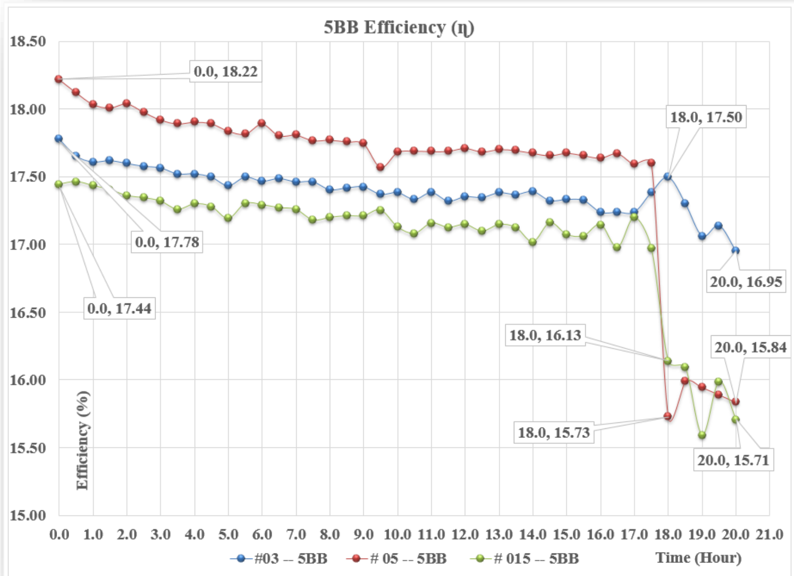

Figure 4: Efficiency curves for all the 5BB solar cell design type

Figs. 17 and 18 show the effective lifetime trending with exposure time every 30 minutes for 18 hours. They also show the effective lifetime after 795°C anneal for less than 2 seconds and post-stability exposure for 2 hours.

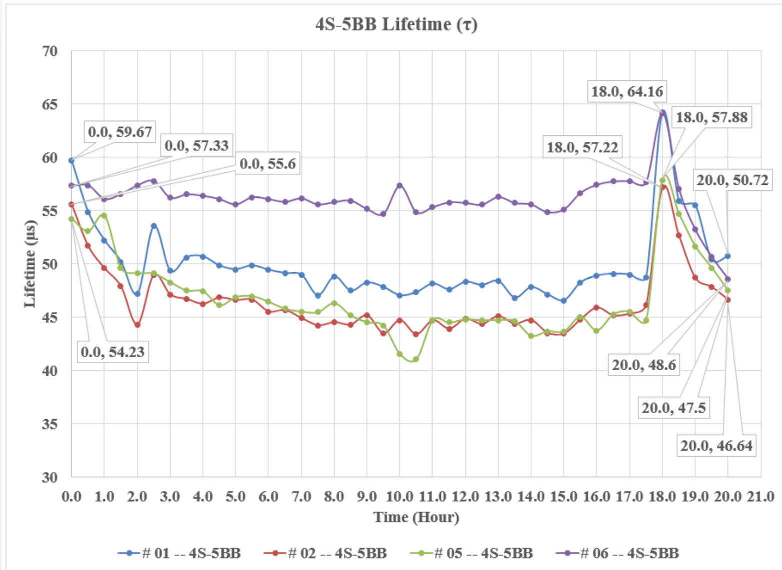

Figure 17: Lifetime curves for all the 4S-5BB solar cell design type

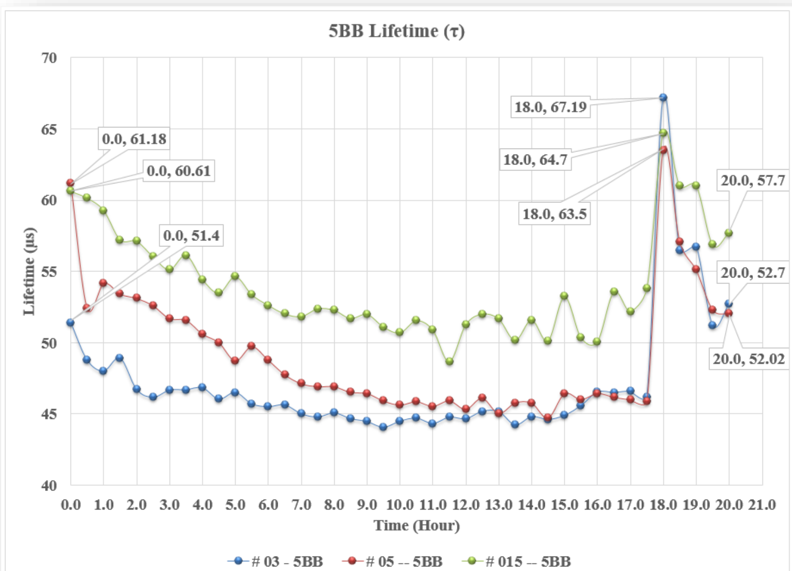

Figure 18: Lifetime curves for all the 5BB solar cell design type

Figs. 19 and 20 show the fill factor trending with exposure time every 30 minutes for 18 hours. They also show the fill factor after 795°C anneal for less than 2 seconds and post-stability exposure for 2 hours.

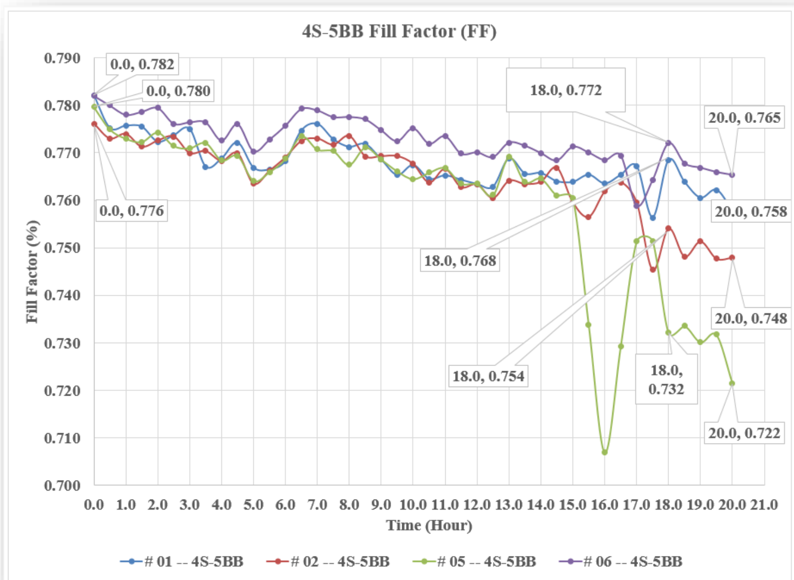

Figure 19: Fill Factor curves for all the 4S-5BB solar cell design type

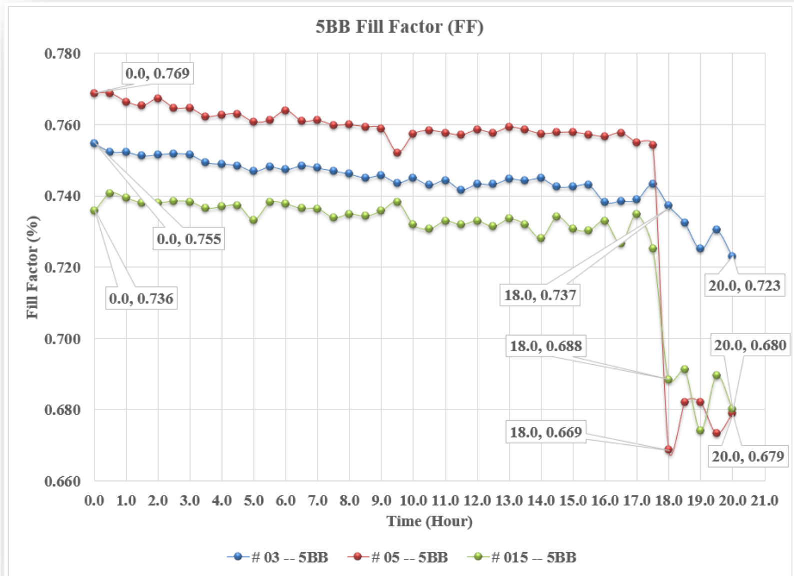

Figure 20:5 Lifetime curves for all the 5BB solar cell design type

Figs. 21 and 22 show the ideality factor trending with exposure time every 30 minutes for 18 hours. They also show the ideality factor after 795°C anneal for less than 2 seconds and post-stability exposure for 2 hours.

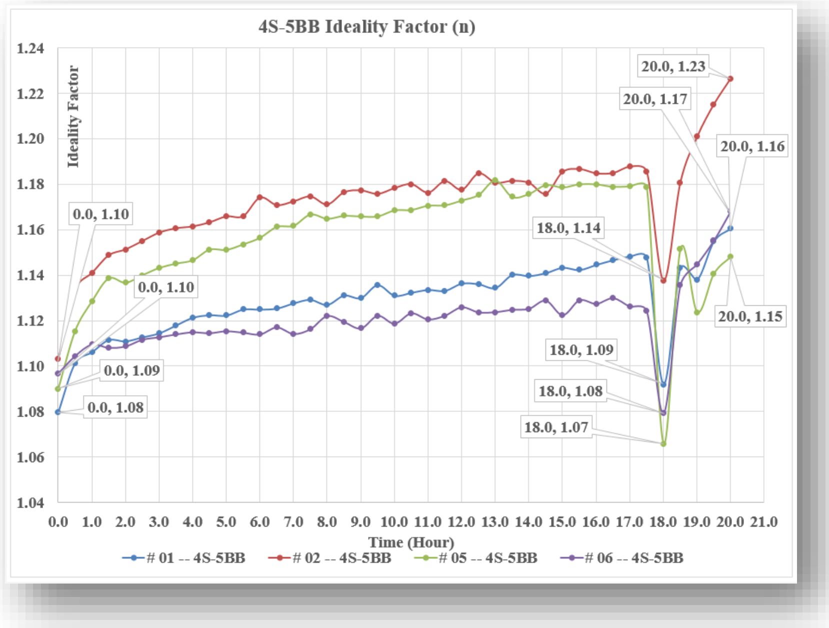

Figure 21: Ideality Factor curves for all the 4S-5BB solar cell design type

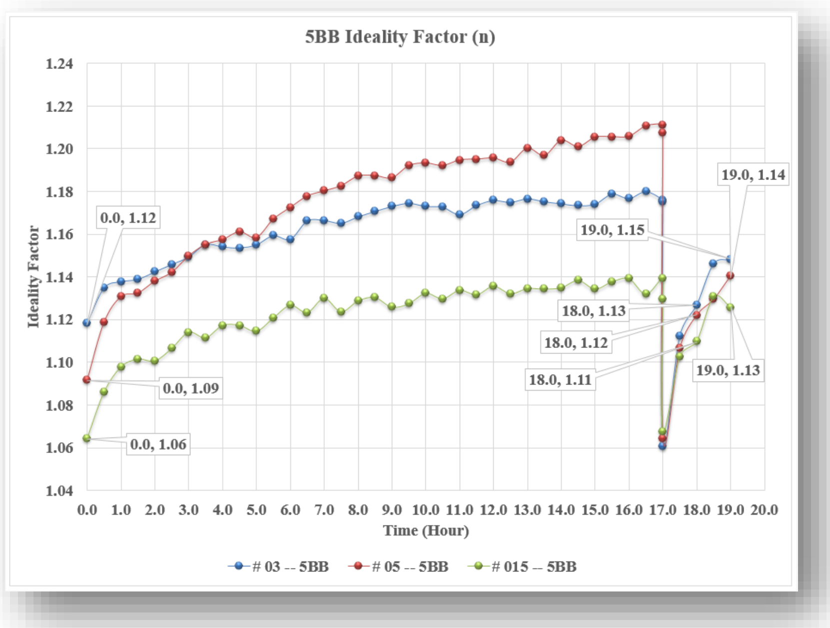

Figure 22: Ideality Factor curves for all the 5BB solar cell design type

Figs. 23 and 24 show the series resistance trending with exposure time every 30 minutes for 18 hours. They also show the series resistance after 795°C anneal for less than 2 seconds and post-stability exposure for 2 hours.

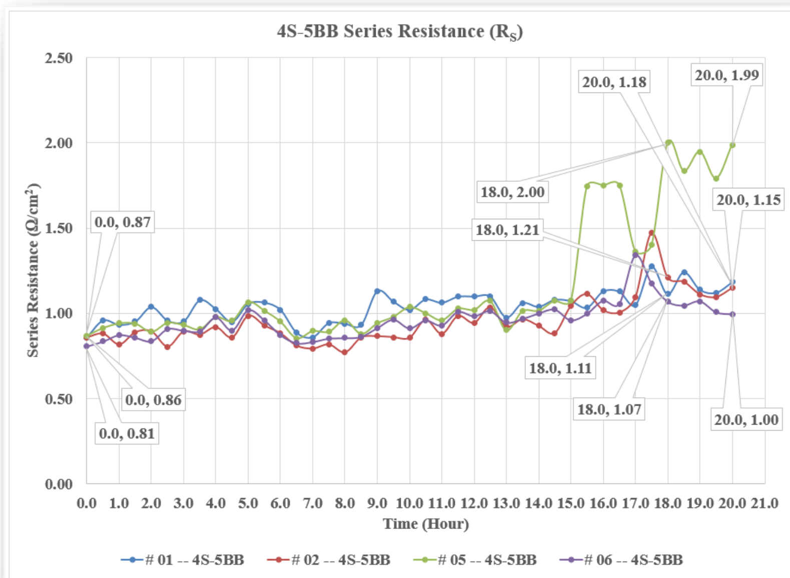

Figure 23: Series resistance curves for all the 4S-5BB solar cell design type

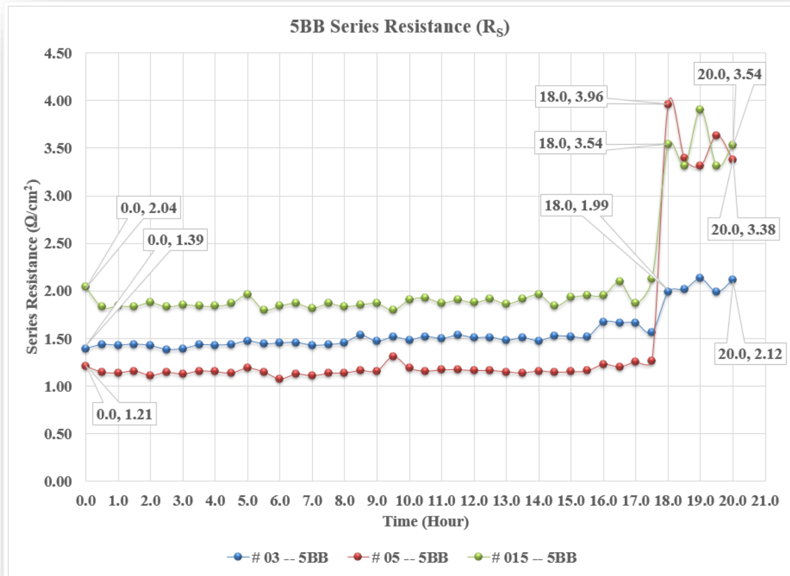

Figure 24: Series resistance curves for all the 5BB solar cell design type

Figs. 25 and 26 show the reverse saturation current trending with exposure time every 30 minutes for 18 hours. They also show the reverse saturation current after 795°C anneal for less than 2 seconds and post-stability exposure for 2 hours.

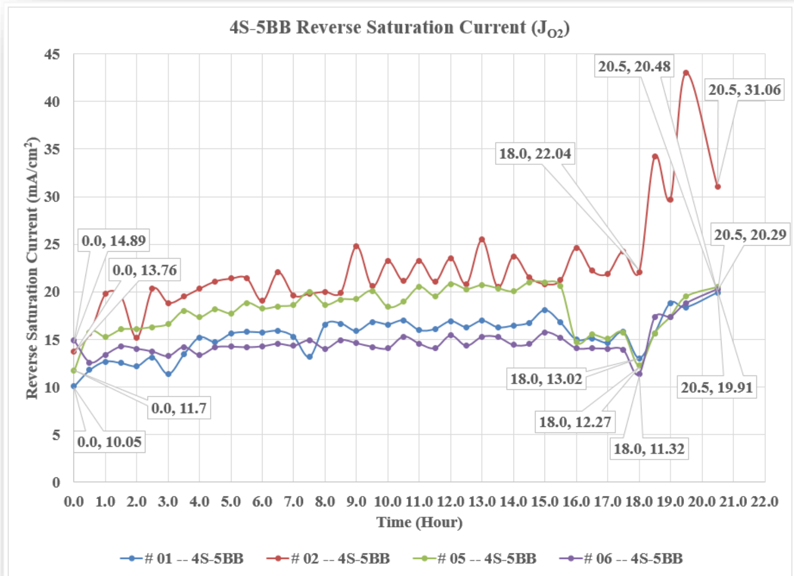

Figure 25: Reverse saturation current curves for all the 4S-5BB solar cell design type

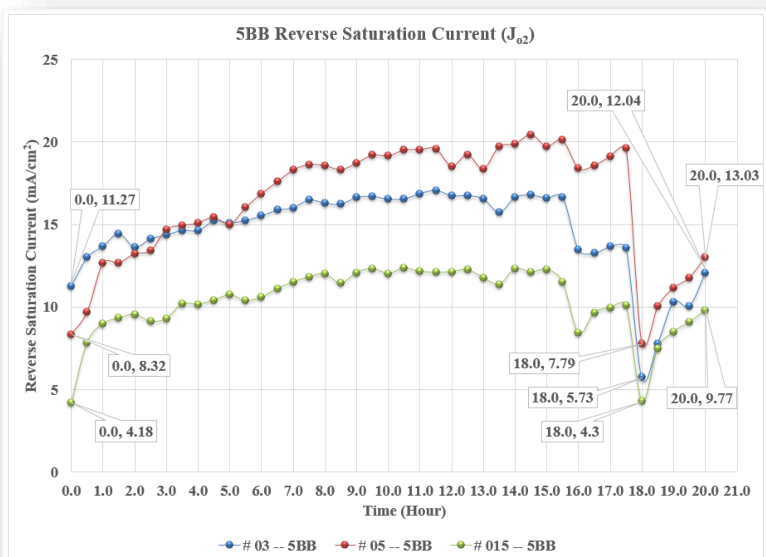

Figure 26: Reverse saturation current curves for all the 5BB solar cell design type

Figs. 27 and 28 show short-circuit current trending with exposure time every 30 minutes for 18 hours. They also show the short-circuit current after 795°C anneal for less than 2 seconds and post-stability exposure for 2 hours.

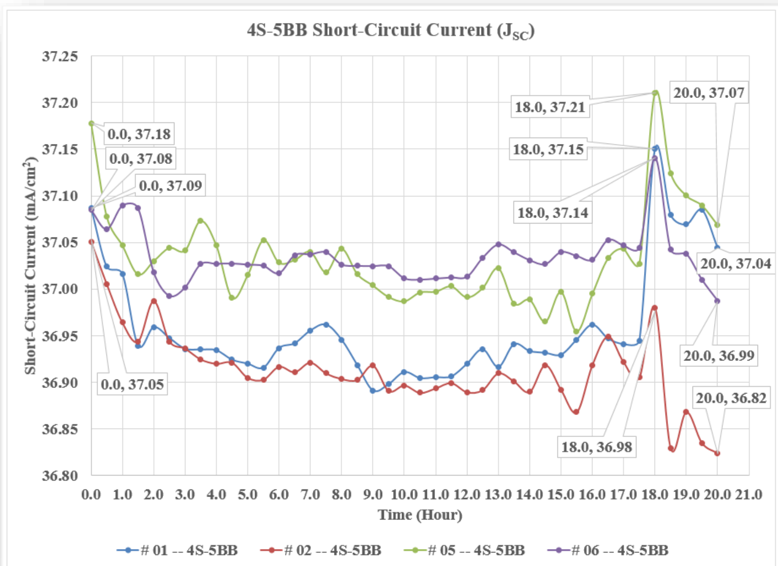

Figure 27: Short-circuit current curves for all the 4S-5BB solar cell design type

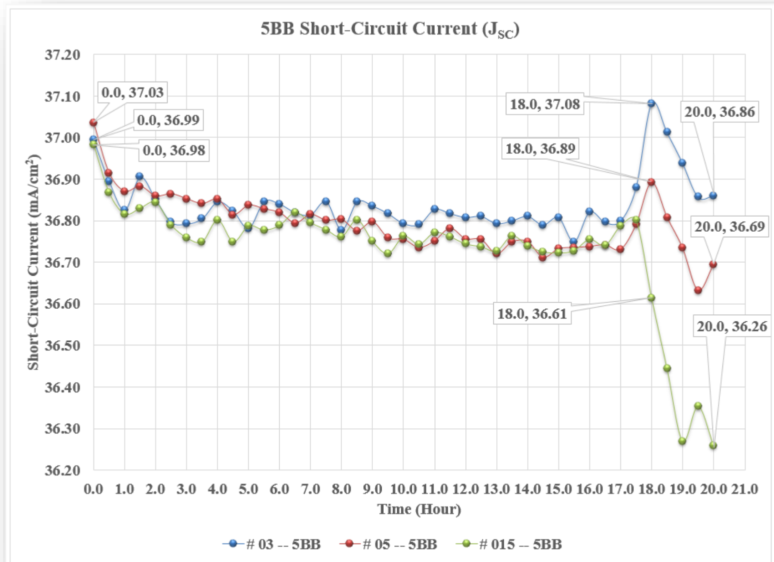

Figure 28: Short-circuit current curves for all the 4S-5BB solar cell design type

Figs. 29 and 30 show the efficiency trending with exposure time after every 30 minutes for 18 hours. They also show the open-circuit voltage after 795°C anneal for less than 2 seconds and post-stability exposure for 2 hours.

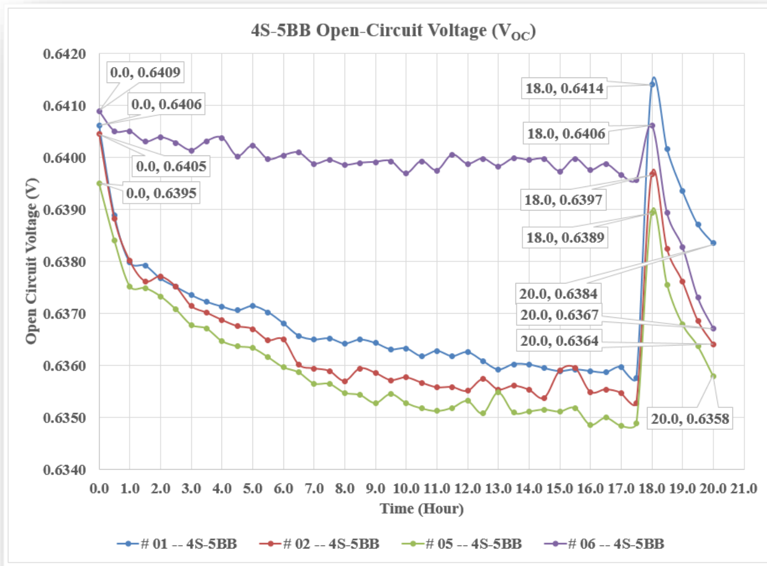

Figure 29: Open-circuit voltage curves for all the 4S-5BB solar cell design type

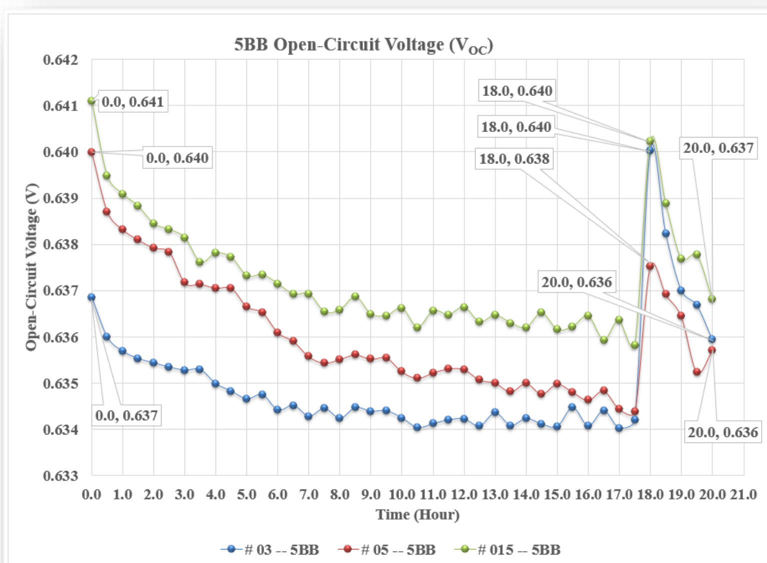

Figure 30: Open-circuit voltage curves for all the 5BB solar cell design type

4.2. Discussion

In order to fully interpret the results from the experiment, a theoretical modeling program for solar cells, Personal Computer One-Dimensional (PC1D) [32], is used to model the effect of bulk lifetime on the efficiency of a silicon solar cell and serve as proof of concept.

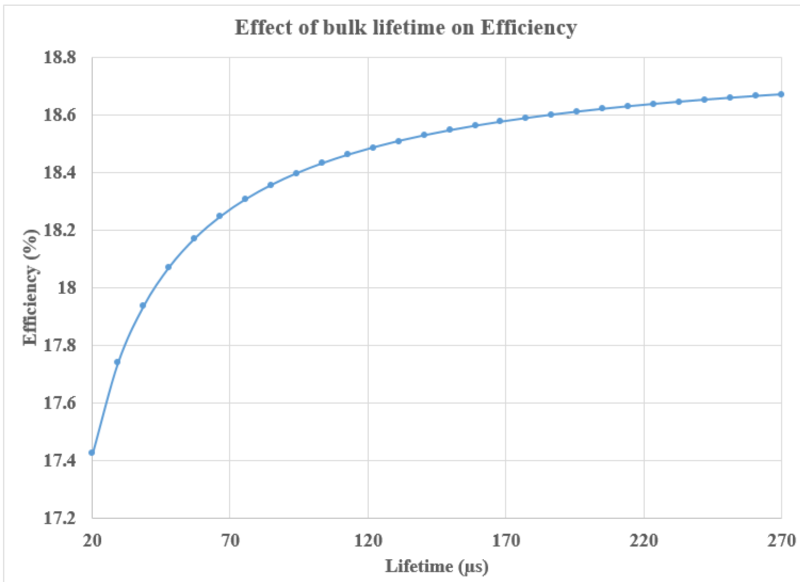

Figure 31: Modeling bulk lifetime impact on solar cell efficiency using PC1D

Fig. 31 shows the effect of changing lifetime on efficiency of the actual solar cells, as listed in Table 2. It should be noted that all the cells used in the experiment, 4S-5BB and 5BB design types, have similar efficiency. Therefore, the impact on one would be similar on the others. Since efficiency is the product of V_{oc}, J_{sc}, and FF, similar graphs are shown in Figs 32, 33, and 34 for V_{oc}, J_{sc}, and FF, respectively.

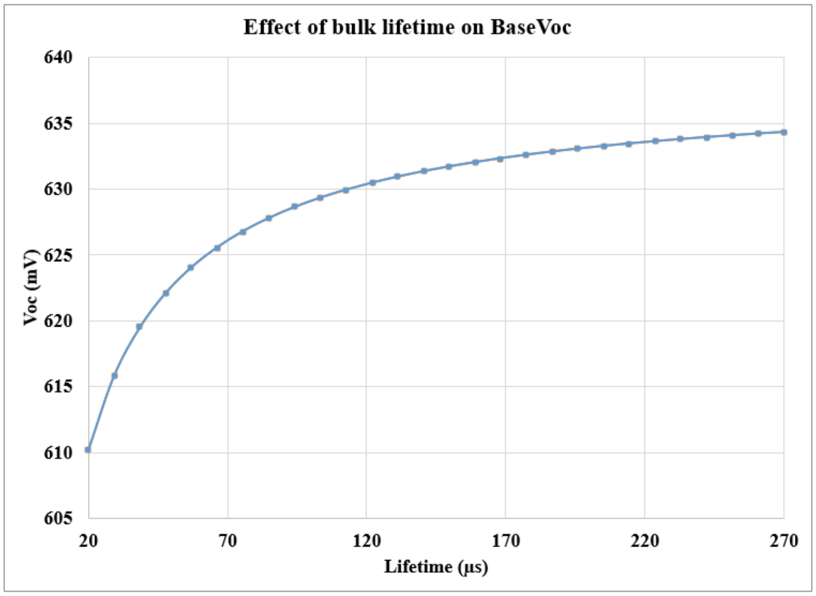

Figure 32: Modeling bulk lifetime impact on solar cell open-circuit voltage using PC1D

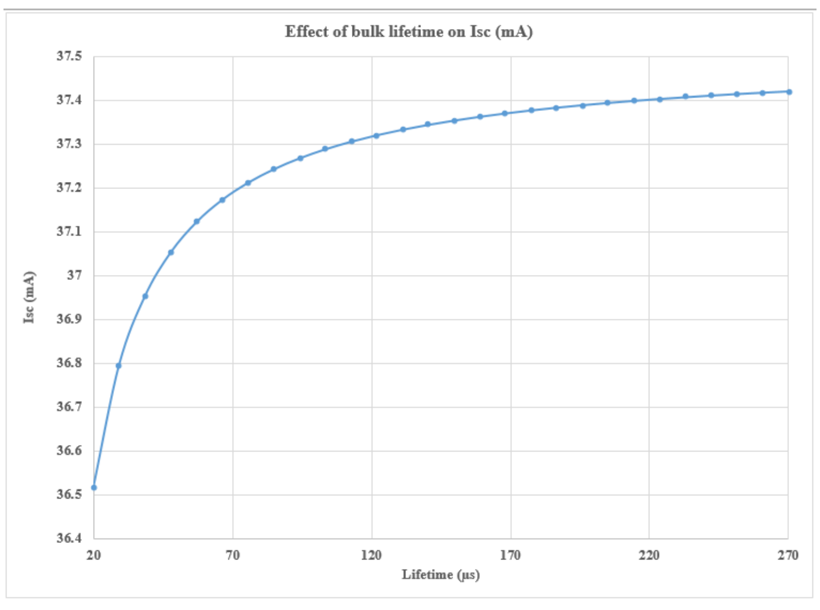

Figure 33: Modeling bulk lifetime impact on solar cell short-circuit current using PC1D

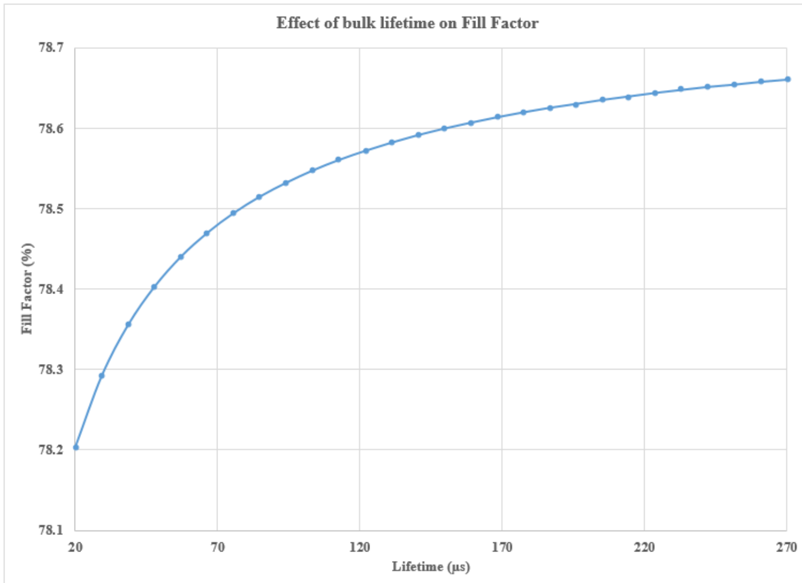

Figure 34: Modeling bulk lifetime impact on solar cell fill factor using PC1D

Figs. 31 – 34 show that an increase in lifetime results in an increase in electrical output parameters as well. The concept of LID is proven since a decreasing trend in lifetime causes a decrease in the electrical output parameters, as shown in Fig. 35, for efficiency.

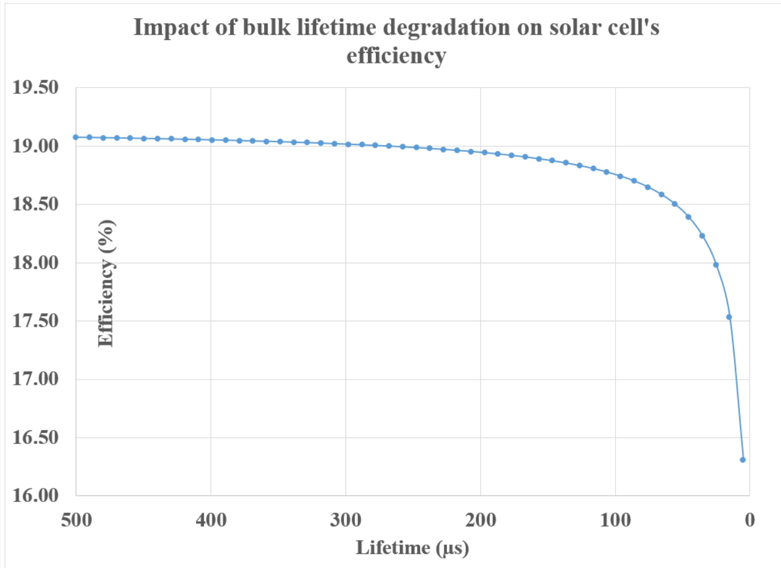

Figure 35: Impact of bulk lifetime on solar cell's efficiency

Experimental results for electrical output parameters, of all solar cells samples shown in Figs. 15 through 30, were summarized in three phases as follows,

- Phase I: Degradation (parameter values measured at time zero and at time 17 hours)
- Phase II: Recovery (parameter values measured immediately after RTP annealing, at time 18)
- Phase III: Stability (last measurement taken post-phase II)

Since all the results have similar trend, only four tables are used for the discussion. Tables 4 and 5 relate to solar cell samples 4S-5BB #002 and 4S-5BB #006, respectively, while Tables 6 and 7 relate to solar cell samples 5BB #003 and 5BB #015, respectively.

Table 4: Three phases parameters monitoring - #002 sample

4S-5BB, #002	Phase I: Degradation		Phase II: Recovery			Phase III: Stability		
			RTP	Diff. (%)	Diff. (%)	Stability	Diff. (%)	Diff. (%)
Parameters	Initial	Final	Anneal	Initial	Final	Post-anneal	initial	RTP anneal
Lifetime (μs)	55.6	45.34	57.22	2.831	20.76	46.64	-19.21	-22.68
V_{oc} (mV)	640.46	635.47	639.68	-0.12	0.66	636.41	-0.64	-0.51
I_{sc} (mA)	37.05	36.92	36.98	-0.19	0.16	36.82	-0.62	-0.43
FF (%)	77.61	75.95	75.4	-2.93	-0.73	74.79	-3.77	-0.82
Efficiency (%)	18.42	17.82	17.84	-3.25	0.11	17.53	-5.08	-1.77
Time (Hour)	0	17	18	0	17	20	0	18

The bulk lifetime for 4S-5BB #002 in Table 4 an absolute lifetime recovery of 102.83% after RTP anneal. However, the efficiency for the same sample, decreased 3.25% at the same time. It is worth to note here that there was 101.1% relative recovery in efficiency due to RTP anneal.

Table 5: Three phases parameters monitoring - #006 sample

4S-5BB, #006	Phase I: Degradation		Phase II: Recovery			Phase III: Stability		
			RTP	Diff. (%)	Diff. (%)	Stability	Diff. (%)	Diff. (%)
Parameters	Initial	Final	Anneal	Initial	Final	Post-anneal	initial	RTP anneal
Lifetime (μs)	57.33	57.77	64.16	10.65	9.96	48.6	-17.96	-32.02
V_{oc} (mV)	640.89	639.67	640.62	-0.04	0.15	636.72	-0.65	-0.61
I_{sc} (mA)	37.08	37.05	37.14	0.16	0.24	36.98	-0.27	-0.43
FF (%)	78.2	75.88	77.2	-1.30	1.71	76.53	-2.18	-0.88
Efficiency (%)	18.59	17.98	18.37	-1.20	2.12	18.02	-3.16	-1.94
Time (Hour)	0	17	18	0	17	20	0	18

Similar observations for 4S-5BB #002, in Table 4, are also made for samples 4S-5BB# 006 and 5BB #003 in Tables 5 and 6, respectively.

Table 6: Three phases parameters monitoring - #003

5BB, #003	Phase I: Degradation		Phase II: Recovery			Phase III: Stability		
			RTP	Diff. (%)	Diff. (%)	Stability	Diff. (%)	Diff. (%)
Parameters	Initial	Final	Anneal	initial	final	Post-anneal	initial	RTP anneal
Lifetime (μs)	51.4	46.58	67.19	23.5	30.67	52.7	2.47	-27.50
V_{oc} (mV)	636.85	634.02	640.01	0.494	0.936	635.94	-0.14	-0.64
I_{sc} (mA)	36.99	36.8	37.08	0.243	0.755	36.86	-0.35	-0.60
FF (%)	75.46	73.88	73.72	-2.36	-0.22	72.31	-4.36	-1.95
Efficiency (%)	17.78	17.24	17.5	-1.6	1.486	16.95	-4.90	-3.24
Time (Hour)	0	17	18	0	17	20	0	18

Although sample 5BB #015 in Table 7 has an absolute lifetime recovery of 106.32%, and a relative lifetime recovery of 119.34%, however, there was no efficiency recovery recorded at all. This results from the contact overfiring as manifested in high series resistance and low fill factor, as shown in Table 8 and Tables 5 through 7, respectively. This also suggests that the peak annealing temperature needs to be optimized, either by decreasing the temperature or increasing the belt speed of RTP.

Table 7: Three phases parameters monitoring - #015

5BB, #015	Phase I: Degradation		Phase II: Recovery			Phase III: Stability		
			RTP	Diff. (%)	Diff. (%)	Stability	Diff. (%)	Diff. (%)
Parameters	Initial	Final	Anneal	initial	final	Post-anneal	initial	RTP anneal
Lifetime (μs)	60.61	52.19	64.7	6.32	19.34	57.7	-5.04	-12.13
V_{oc} (mV)	641.09	636.36	640.23	-0.13	0.60	636.81	-0.67	-0.54
I_{sc} (mA)	36.98	36.78	36.61	-1.01	-0.46	36.25	-2.01	-0.99
FF (%)	73.57	73.47	68.82	-6.90	-6.76	68.02	-8.16	-1.18
Efficiency (%)	17.44	17.2	16.13	-8.12	-6.63	15.7	-11.08	-2.74
Time (Hour)	0	17	18	0	17	20	0	18

Similar observations are made for the rest of solar cell samples used in the experiment.

Since the efficiency can be impacted by low fill factor, the parameters that affect fill factor were investigated.

Table 8: Critical solar cell parameters 4S-5BB

Critical solar cell parameters					
Cell ID		4 Street - 5 Busbars (4S-5BB)			
		#001	**#002**	**#005**	**#006**
Parameters		Values	Values	Values	Values
R_{series} (Ω-cm2)	**Stability (final)**	1.18324765	1.1489	1.98899275	0.995202013
	Pre-Degradation (initial)	0.8587	0.8584	0.8696	0.8067
	Difference	0.32454765	0.2905	1.11939275	0.188502013
J_{o2} (mA/cm^2)	**Stability (final)**	19.91	31.06	20.48	20.29
	Pre-Degradation (initial)	10.05	13.76	11.7	14.89
	Difference	9.86	17.3	8.78	5.4
J_{sc} (mA/cm^2)	**Stability (final)**	0.03704	0.03682	0.03706803	0.036987521
	Pre-Degradation (initial)	0.037338	0.03705	0.037178	0.037084
	Difference	-0.000298	-0.00023	-0.00011	-9.6479E-05
Ideality Factor (n)	**Stability (final)**	1.16061083	1.22656	1.14816997	1.1681
	Pre-Degradation (initial)	1.079	1.103	1.089	1.097
	Difference	0.08161083	0.12356	0.05916997	0.0711

Those parameters include series resistance, ideality factor, and reverse saturation current density. Table 8 and 9 contain values for these parameters comparing, side-by-side, the pre-degradation and stability.

Table 9: Critical solar cell parameters 5BB

Critical solar cell parameters				
Cell ID		5 Busbars (5BB)		
		#003	#005	#015
Parameters		Values	Values	Values
R_{series} (Ω-cm2)	Stability (final)	2.11681734	3.37795	3.53585414
	Pre-Degradation (initial)	1.391961	1.2084	2.0419496
	Difference	0.72485634	2.16955	1.49390454
J_{o2} (mA/cm^2)	Stability (final)	12.04	13.03	9.77
	Pre-Degradation (initial)	11.27	11.27	4.18
	Difference	0.77	1.76	5.59
J_{sc} (mA/cm^2)	Stability (final)	0.03686025	0.03669	0.03625907
	Pre-Degradation (initial)	0.036993	0.03703	0.036982
	Difference	-0.0001327	-0.00034	-0.0007229
Ideality Factor (n)	Stability (final)	1.14809575	1.14043	1.12572719
	Pre-Degradation (initial)	1.118	1.092	1.064
	Difference	0.03009575	0.04843	0.06172719

The highlighted column in Table 8 (#002) for the 4S-5BB design type indicates the solar cell sample that was analyzed and column in Table 9 (#003) for the 5BB design type, similarly.

CHAPTER 5: CONCLUSION AND FUTURE SCOPE

5.1. Conclusion

For sustainable and low cost solar electricity, the longevity of solar cell is critical. This calls for stabilized power output from a solar cell. However, a solar cell fabricated on a p-type substrate suffers from degradation immediately it is exposed to sunlight. This thesis addresses a cost-effective method of stabilizing the power output. Although the method adopted in this thesis did not show full recovery, there are lessons to learn. It also opens up a new chapter for further investigations.

It can be concluded from experimental results that:

- Solar cell’s structure (i.e. 4S-5BB vs. 5BB) does not impact the lifetime recovery following degradation. Rather, it is the boron-oxygen pair in the bulk of the material that controls the recovery.
- The fact that the lifetime fully recovered after anneal, suggests that hydrogen retention at the boron-oxygen sites was higher than hydrogen effusion from the material. Thus, the boron-oxygen recombination centers are fully passivated.
- The increase in the series resistance after annealing suggests that the peak temperature should either be decreased or the belt speed be increased. This will also enhance lifetime recovery because of a shorter dwell time at slightly lower temperature. It is worthy to note that, contact firing is very critical to efficiency recovery.

- Because of the non-optimized contact anneal, J_{o2} increases, indicating high junction recombination which decreases fill factor. That is why the efficiency could not be recovered. Since efficiency is a function of fill factor, thus a decrease in fill factor results in lower efficiency.

5.2. Future Scope: Recommendations and Future Work

Although mitigating LID utilizing RTP method is low cost, care must be taken in choosing the anneal temperature after degradation to avoid contact deterioration. Therefore, belt speed and peak firing temperature must be investigated to maximize lifetime and efficiency recovery.

REFERENCES

[1] S. Shafiee and E. Topal, "When will fossil fuel reserves be diminished?," *Energy policy,* vol. 37, pp. 181-189, 2009.

[2] T. F. Garrity, "Innovation and trends for future electric power systems," in *Power Systems Conference, 2009. PSC '09.*, 2009, pp. 1-8.

[3] M. H. Nehrir, C. Wang, K. Strunz, H. Aki, R. Ramakumar, J. Bing*, et al.*, "A Review of Hybrid Renewable/Alternative Energy Systems for Electric Power Generation: Configurations, Control, and Applications," *IEEE Transactions on Sustainable Energy,* vol. 2, pp. 392-403, 2011.

[4] N. R. Baker and J. R. Bowyer, *Photoinhibition of photosynthesis: from molecular mechanisms to the field*: Bios Scientific Publishers, 1994.

[5] BP, "BP Statistical Review of World Energy," ed, 2016, pp. 3 - 4.

[6] John W. Twidell and A. D. Weir, *Renewable Energy Resources*, Second ed. London and New York: Taylor & Francis, 2006.

[7] A. Shah, P. Torres, R. Tscharner, N. Wyrsch, and H. Keppner, "Photovoltaic technology: the case for thin-film solar cells," *science,* vol. 285, pp. 692-698, 1999.

[8] S. Xiao, S. Xu, X. Wang, and Z. Wang, "High-efficiency solar cells: physics, materials, and devices," ed: Springer International Publishing, Switzerland Google Scholar, 2014.

[9] M. A. Green, "Third Generation Photovoltaics: Ultra-high Conversion Efficiency at Low Cost," *Progress in Photovoltaics: Research and Applications,* vol. 9, pp. 123 - 135, 2001.

[10] V. D. D. Valerio Lo Brano, Giovanni Cipriani, "A comparison of different one-diode models for the representation of I-V characteristic of a PV cell," *Elsevier,* vol. 32, pp. 684 - 696, 2014.

[11] R. M. Swanson, "Approaching the 29% limit efficiency of silicon solar cells," *Photovoltaic Specialists Conference, 31th IEEE,* pp. 889 - 894, 2005.

[12] M. A. Green, "Solar cells: operating principles, technology, and system applications," 1982.

[13] B. M. Damiani, "Investigation of light induced degradation in promising photovoltaic grade silicon and development of porous silicon anti-reflection coatings for silicon solar cells," Georgia Institute of Technology, 2004.

[14] R. Crabb, "Photon induced degradation of electron irradiated silicon solar cells," in *Proceedings of the Ninth IEEE Photovoltaic Specialists Conference, Silver Springs*, 1972, pp. 329-330.

[15] H. Fischer and W. Pschunder, "Investigation of photon and thermal induced changes in silicon solar cells," in *Photovoltaic Specialists Conference, 10 th, Palo Alto, Calif*, 1974, pp. 404-411.

[16] H. W. B. V.G. Weizer, J.D. Broder, R.E. Hart, and S.H. Lamneck, "Photon Degradation Effects in Terrestrial Solar Cells," *Journal of Applied Physics*, June 5-8, 1978 1978.

[17] J. Corbett, A. Jaworowski, R. Kleinhenz, C. Pierce, and N. Wilsey, "Photodegradation in silicon," *Solar cells*, vol. 2, pp. 11-22, 1980.

[18] J. Reiss, R. King, and K. Mitchell, "Characterization of diffusion length degradation in Czochralski silicon solar cells," *Applied physics letters*, vol. 68, pp. 3302-3304, 1996.

[19] J. Schmidt, A. G. Aberle, and R. Hezel, "Investigation of carrier lifetime instabilities in Cz-grown silicon," in *Conference Record of the Twenty Sixth IEEE Photovoltaic Specialists Conference - 1997*, 1997, pp. 13-18.

[20] J. Dicker, J. Schumacher, S. Glunz, and W. Warta, "Characterization of high-efficiency silicon solar cells with rear side contacts," in *Proc. 2nd WCPSEC*, 1998, p. 95.

[21] J. Schmidt and A. Cuevas, "Progress in understanding and reducing the light degradation of Cz silicon solar cells," 2000.

[22] T. Saitoh, H. Hashigami, S. Rein, and S. Glunz, "Overview of light degradation research on crystalline silicon solar cells," *Progress in Photovoltaics: Research and Applications*, vol. 8, pp. 537-547, 2000.

[23] S. W. Glunz, S. Rein, J. Y. Lee, and W. Warta, "Minority carrier lifetime degradation in boron-doped Czochralski silicon," *Journal of Applied Physics,* vol. 90, pp. 2397-2404, 2001.

[24] T. K. Vu, Y. Ohshita, K. Araki, and M. Yamaguchi, "Generation and annihilation of boron–oxygen related defects in boron-doped Czochralski-grown Si solar cells," *Journal of applied physics,* vol. 91, pp. 4853-4856, 2002.

[25] J. Schmidt, "Light-induced degradation in crystalline silicon solar cells," in *Solid State Phenomena*, 2004, pp. 187-196.

[26] B. Lim, A. Liu, D. Macdonald, K. Bothe, and J. Schmidt, "Impact of dopant compensation on the deactivation of boron-oxygen recombination centers in crystalline silicon," *Applied Physics Letters,* vol. 95, p. 232109, 2009.

[27] B. Lim, K. Bothe, and J. Schmidt, "Impact of oxygen on the permanent deactivation of boron–oxygen-related recombination centers in crystalline silicon," *Journal of Applied Physics,* vol. 107, p. 123707, 2010.

[28] M. H. Kang, J. Hong, I. Cooper, A. Ebong, B. Rounsaville, and A. Rohatgi, "Reduction in light induced degradation (LID) in B-doped Cz-Si solar cells with SiCxNy antireflection (AR) coating," *Journal of The Electrochemical Society,* vol. 158, pp. H724-H726, 2011.

[29] B. Sopori, P. Basnyat, S. Devayajanam, S. Shet, V. Mehta, J. Binns*, et al.*, "Understanding light-induced degradation of c-Si solar cells," in *Photovoltaic Specialists Conference (PVSC), 2012 38th IEEE*, 2012, pp. 001115-001120.

[30] A. Ebong, N. Chen, A. Chowdhury, and V. Unsur, "The impact of rapid thermal processing (RTP) on crystalline silicon solar cell performance and light induced degradation (LID)," in *Photovoltaic Specialist Conference (PVSC), 2015 IEEE 42nd*, 2015, pp. 1-4.

[31] N. Chen, "Understanding and Development of cost-effective industrial aluminum back surface field (Al-BSF) silicon solar cells," PhD, Electrical Engineering UNC Charlotte, 2015, 2015.

[32] D. T. R. P.A. Basore, and A.W. Smith, "PC-1D version 2: enhanced numerical solar cell modeling," *Conf. Proc. 20th, Photovoltaic Specialists Conference,* 26 - 30 September 1988 1988.